AJNR

Cranial CT of autosomal recessive osteopetrosis.

W S Bartynski, P D Barnes and J K Wallman

AJNR Am J Neuroradiol 1989, 10 (3) 543-550
http://www.ajnr.org/content/10/3/543

Cranial CT of Autosomal Recessive Osteopetrosis

Walter S. Bartynski[1,2]
Patrick D. Barnes[1]
James K. Wallman[1,3]

Eight infants with radiographic and bone biopsy evidence of autosomal recessive osteopetrosis were evaluated by cranial CT. The clinical presentations and CT characteristics support the theory that this disorder exhibits severe and mild variants. At an early stage the severe variant demonstrates small optic canals, small orbits with proptosis, and a small nasoethmoid complex without significant bone thickening. The paranasal sinuses show bud formation but no pneumatization. The temporal bone retains a fetal appearance with trumpet-shaped internal auditory canals, prominent subarcuate fossae, and no mastoid pneumatization. The ventricles and subarachnoid spaces are enlarged. Bone thickness increases with age, leading to further orbital encroachment. Similar but less severe features are present in the mild variant.

Underdevelopment of the orbits, nasoethmoid complex, and temporal bone suggests that delayed maturation is the primary morphologic abnormality of the skull base in osteopetrosis, and that bone thickening is a secondary manifestation caused by reduced bone turnover.

Osteopetrosis is a genetic disorder that occurs in either a rare autosomal recessive form (malignant, congenital, precocious) or the more common autosomal dominant form (benign, tarda, adult) [1]. Patients with the recessive form develop progressive marrow-space encroachment with small neural foramina, which likely result from inadequate osteoclastic bone resorption [2]. These infants develop anemia, extramedullary hematopoiesis, susceptibility to infection, and multiple cranial nerve palsies. The characteristic plain film findings in the malignant form have been described [1, 3]. This report focuses on the cranial CT features to detail the anatomic alterations and to describe a third, "mild," form of autosomal recessive osteopetrosis.

Materials and Methods

Eight infants with autosomal recessive osteopetrosis were evaluated with cranial CT at The Children's Hospital between April 17, 1981 and July 6, 1986. A retrospective review of the medical records and CT scans forms the basis of this report. The diagnosis of autosomal recessive osteopetrosis was based on clinical presentation, characteristic radiographic findings, and bone biopsy. All patients were referred for advanced treatment, including hormonal therapy (vitamin D and/or calcitriol) and consideration for bone marrow transplantation [4, 5].

Cranial CT scans were acquired on a GE 8800 or 9800 CT/T system. Studies were requested primarily to evaluate complications of osteopetrosis—such as increasing head circumference, altered neurologic status (orbital, optic foraminal)—and/or to perform temporal bone examination for cranial nerve dysfunction. Cranial CT sections were obtained parallel to the Reid baseline at 5–10-mm slice thickness. Orbital sections were obtained parallel to the inferior orbitomeatal line with 1.5–3-mm slice thickness. Temporal bone sections were obtained parallel to the canthomeatal line with 1.5–3-mm thickness. Sedation when necessary included either chloral hydrate, 50 mg/kg, orally, or a mixture of Demerol 25 mg, Phenergan 6.5 mg, and Thorazine 6.25 mg/ml (1 ml per 15 kg IM; maximum, 2 ml).

Received June 29, 1987; accepted after revision September 9, 1988.

Presented at the annual meeting of the American Society of Neuroradiology, New York, May 1987.

[1] Department of Radiology, The Children's Hospital, Boston, MA 02115.

[2] Present address: Department of Radiology, The Western Pennsylvania Hospital, 4800 Friendship Ave., Pittsburgh, PA 15224. Address reprint requests to W. S. Bartynski.

[3] Present address: Department of Radiology, Lahey Clinic Medical Center, Burlington, MA 01805.

AJNR **10:543–550, May/June 1989**
0195–6108/89/1003–0543

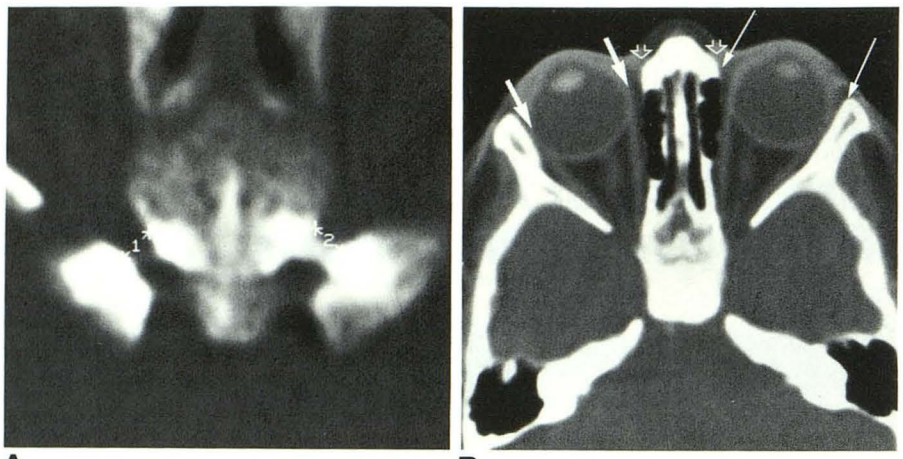

Fig. 1.—*A*, Cursors deposited along medial and lateral walls of both optic canals in a wide-window, bone-targeted image. Distance is measured by using the GE "measure distance" keyboard function.

***B*, Normal patient at 9 months of age. Interorbital distance (*open arrows*), orbital rim transverse diameters (*thin arrows*), and globe transverse diameters (*wider arrows*) were measured by ruler between the indicated locations. Distances were calculated by multiplying these distances by the magnification factor, determined by measuring the raster scale of same image.**

Orbital rim transverse diameters, globe transverse diameters, interorbital distance, and optic canal diameters were measured on intermediate or wide window axial images of five patients in which appropriate views of the orbits were available (cases 2–6). In three of our patients (cases 1, 7, and 8), orbital studies were not performed. Optic canals were measured by utilizing the distance function of the GE system after cursor deposition on the medial and lateral canal wall (Fig. 1A). Orbital rim diameters, globe diameters, and interorbital distances were measured retrospectively (Fig. 1B). Interorbital distance was measured at the level of the dacryon. Transverse orbital rim diameters were recorded as the widest distance between the medial and lateral orbital rim in a series of contiguous orbital images. Globe transverse diameters were recorded as the widest distance between the peripheral limits of the globe, taking the line perpendicular to the orbital axis. These retrospective dimensions were obtained by measurement with a millimeter-scale ruler and application of the appropriate magnification factor after measuring the raster scale on the same image. We estimate the standard deviation of these measurements, by this technique, to be approximately ± 1 ml. Normal values for age are available for comparison [6–9].

Four children (ages 13 days, 2 months, 4 months, and 1 year, respectively) had only one CT examination while four others (age range, 1–23 months) were examined on at least three occasions.

Results

All patients were younger than 6 months old at time of presentation (Table 1), and all had radiographic and iliac bone biopsy findings consistent with osteopetrosis. There were six

TABLE 1: Clinical Findings in Autosomal Recessive Osteopetrosis

Case No.	Age (months)	Presenting Findings				Visual		Auditory	
		Clinical	Form	Head Circumference (percentile)	Hemato-poietic	Clinical	VER	Clinical	BSAER
1	2	Decreased visual responses	Severe	98	A, H, T	No visual responses	Optic nerve dysfunction	Otitis	CHL & SNHL
2	2	Decreased visual responses	Severe	98	A, H	No visual responses, optic atrophy	Optic nerve dysfunction	Mild hearing loss but responded to sound	SNHL
3	5	Infection, family history	Severe	97	A, H	Normal	Normal	Otitis	CHL
4	1	Family history	Severe	90	A, H	Mild optic atrophy	Normal	Frequent otitis	CHL
5	5	Fracture, dysmorphic	Severe	50	A, H, T	Optic atrophy	Optic nerve dysfunction	Responded to sound	CHL & SNHL
6	1	Infection	Severe	97	A, H	Normal	Normal	Frequent otitis	Normal
7	1	Infection, increasing head circumference	Mild	98	H	Normal	Normal	Frequent otitis	Normal
8	4	Increasing head circumference	Mild	95	H	Normal	Normal	Frequent otitis	Normal

Note.—VER = visual evoked responses, BSAER = brainstem auditory evoked responses, A = anemia, H = hepatomegaly, T = thrombocytopenia, CHL = conductive hearing loss, SNHL = sensorineural hearing loss.

boys and two girls, and two patients had a positive family history. Two subpopulations (severe and mild) of recessive osteopetrosis were identified.

Severe Form

Clinical

Six of eight children developed severe and rapidly progressing complications of osteopetrosis related to bone marrow and skull base foraminal involvement. Moderate to severe anemia, hepatosplenomegaly, and extramedullary hematopoiesis were present initially in all six infants, while intermittent thrombocytopenia was an additional finding in two of these infants. Three children had severe visual impairment with roving eye movements. Visual evoked responses correlated with clinical optic atrophy. Otitis media was common. Auditory evoked responses, although difficult to test, were abnormal in five. Sensorineural hearing loss was the dominant feature in two, while a nonspecific element of conductive loss was present in three. One child suffered moderate anemia without visual or auditory symptoms. Facial nerve dysfunction was suspected in two. Five of the six had progressive head enlargement with circumferences at or above the 90th percentile. CT abnormalities in this group were divided into five categories, as follows.

Radiologic

1. *Facial bones*

A spectrum of findings was observed, including increased medullary density of the maxilla, sphenoid, and zygoma with reduced trabecular definition, loss of corticomedullary interfaces, and absence of pneumatization (Figs. 2 and 3). These findings were more severe with increasing age. The ethmoid air cells were underdeveloped, containing fluid or thickened mucosa. The nasal cavity and the ethmoid complex appeared small in width, particularly posteriorly, while the anterior interorbital distance was increased for age in five patients (Table

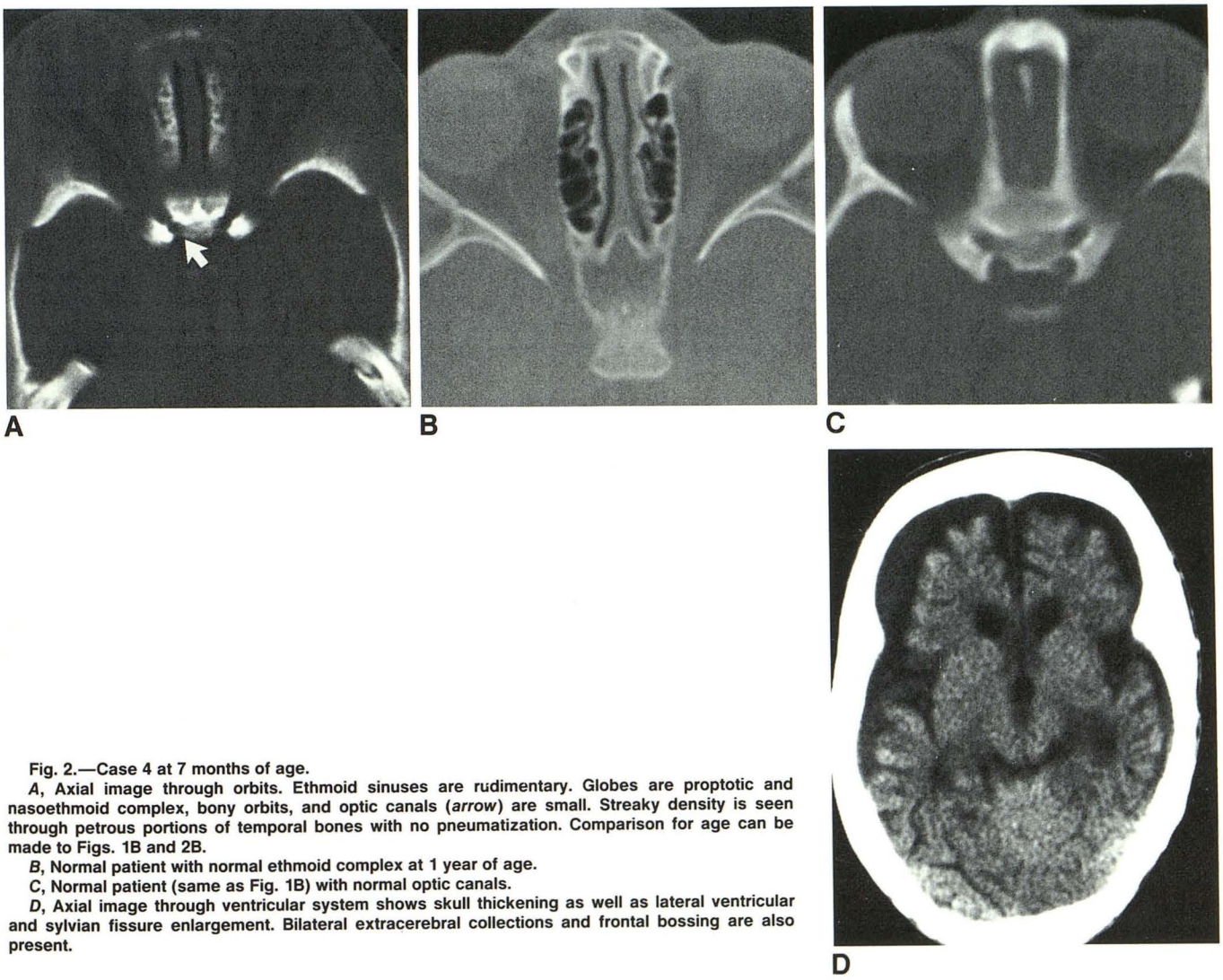

Fig. 2.—Case 4 at 7 months of age.

***A*, Axial image through orbits. Ethmoid sinuses are rudimentary. Globes are proptotic and nasoethmoid complex, bony orbits, and optic canals (*arrow*) are small. Streaky density is seen through petrous portions of temporal bones with no pneumatization. Comparison for age can be made to Figs. 1B and 2B.**

***B*, Normal patient with normal ethmoid complex at 1 year of age.**

***C*, Normal patient (same as Fig. 1B) with normal optic canals.**

***D*, Axial image through ventricular system shows skull thickening as well as lateral ventricular and sylvian fissure enlargement. Bilateral extracerebral collections and frontal bossing are also present.**

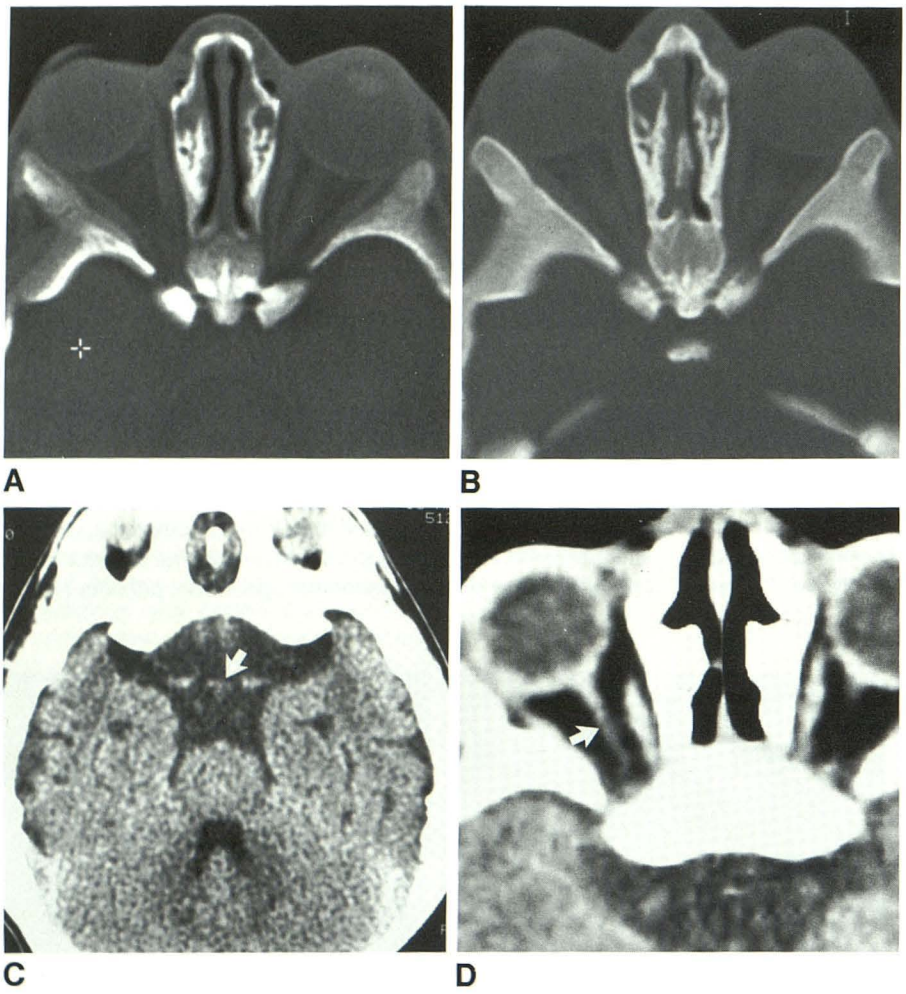

Fig. 3.—*A*, Axial image through orbits of case 2 at 4 months of age. Despite minimal bone thickening, optic canals and orbits are small with proptosis already apparent. Wide angle of orbital axes is caused by increased interorbital distance and small nasoethmoid complex. Ethmoid sinuses are rudimentary.

***B*, Axial image through orbits of case 2 at 16 months of age. There is marked bone thickening with loss of trabecular pattern and increased bone density. Optic canal diameters remain unaltered despite bone thickening. Ethmoid sinuses remain rudimentary. There is straightening of sigmoid shape to lateral orbital walls.**

***C*, Axial image through suprasellar cistern of case 2 at 16 months of age. Atrophy of optic chiasm (*arrow*) is seen between internal carotid arteries and anterior to infundibulum. Suprasellar cistern and both temporal horns are enlarged.**

***D*, Axial image through orbits of case 4 shows intraorbital optic nerve thinning (*arrow*) caused by optic nerve atrophy.**

TABLE 2: Orbital Measurements in Selected Cases

Case No.	Age (months)	Globe Diameter (mm)	Transverse Orbital Diameter (mm)	Interorbital Distance (mm)	Optic Foramen	
					L (mm)	R (mm)
2	4	21	24	17.5	2.4	2.4
	12	24	26	19	2.5	2.5
	16	24	27	19	2.5	2.5
	18	24	28	19	2.5	2.5
3	12	25	30	26	2.5	2.5
4	1	17	22	20	1.5	2.0
	7	22	27	23	2.5	2.7
5	2	20	25	26	1.5	1.5
6	4	18.5	25	22.5	3.2	2.9

Normal values: Globe diameters, transverse (7) —Birth: 12.5–17 mm
Adult: 17.9–23.5 mm
Globe diameter, transverse (9) —Adult: 24.13 mm
Orbital rim diameter, transverse (8)—Adult: 24.13 mm
Fetus (8 mo): 18 mm
Newborn (6 mo): 27 mm
Child (7 yr): 33 mm
Interorbital distance (6) —1 year: 16 mm
2 years: 18 mm; Range, 15–21 mm
Optic canal diameter (6) —Neonate: 4 mm
Infant (6 mo): 5 mm
Child (3–5 yr): 5.5 mm

2). This resulted in a characteristic appearance of posterior nasoethmoidal narrowing and interorbital widening anteriorly. Increased interorbital distance for age was present in all five children in whom measurements were obtained.

2. *Orbits*

Exophthalmos and relative bony orbital encroachment progressed with age. Early in life the orbits appeared small in size despite globe diameters and orbital rim diameters remaining within or slightly exceeding the upper limits of normal (Table 2). Clinical hypertelorism was present in all patients, and increased interorbital distances were noted in the five patients in whom measurements were obtained. Proptosis was noted early, although only mild bone thickening was present yet (Fig. 3). Bone thickening of the zygoma and sphenoid progressed, causing loss of the normal sigmoid shape of the lateral orbital wall (Fig. 3). The optic canals were small bilaterally in five patients (Table 2). Optic nerve thinning was occasionally noted, intraorbitally and intracranially, suggesting atrophy (Figs. 3C and 3D). The reduced posterior ethmoid width along with increased interorbital distances resulted in what appears to be an increased angle of intersection of the orbital axes in all patients.

3. *Temporal bone*

The petrous portions appeared small and nonpneumatized (Fig. 4). Increased mastoid density with low-density streaking was seen (lack of septation). Prominent subarcuate fossae were consistently identified with deep grooves extending into the region of the superior semicircular canals (Figs. 4 and 5). The middle ear cavity was small with intact ossicles, small attic, and no antrum. The otic capsule was normally hyperdense, with the cochlea, vestibule, and semicircular canals of normal size and orientation. The facial nerve canal was never identified, although the stylomastoid foramen was occasionally seen (Fig. 4). The external auditory canal appeared normal. The internal auditory canal appeared shortened with an exaggerated trumpet shape: small diameter laterally, large diameter medially (Fig. 4). This configuration obscured reference points for measuring canal dimensions.

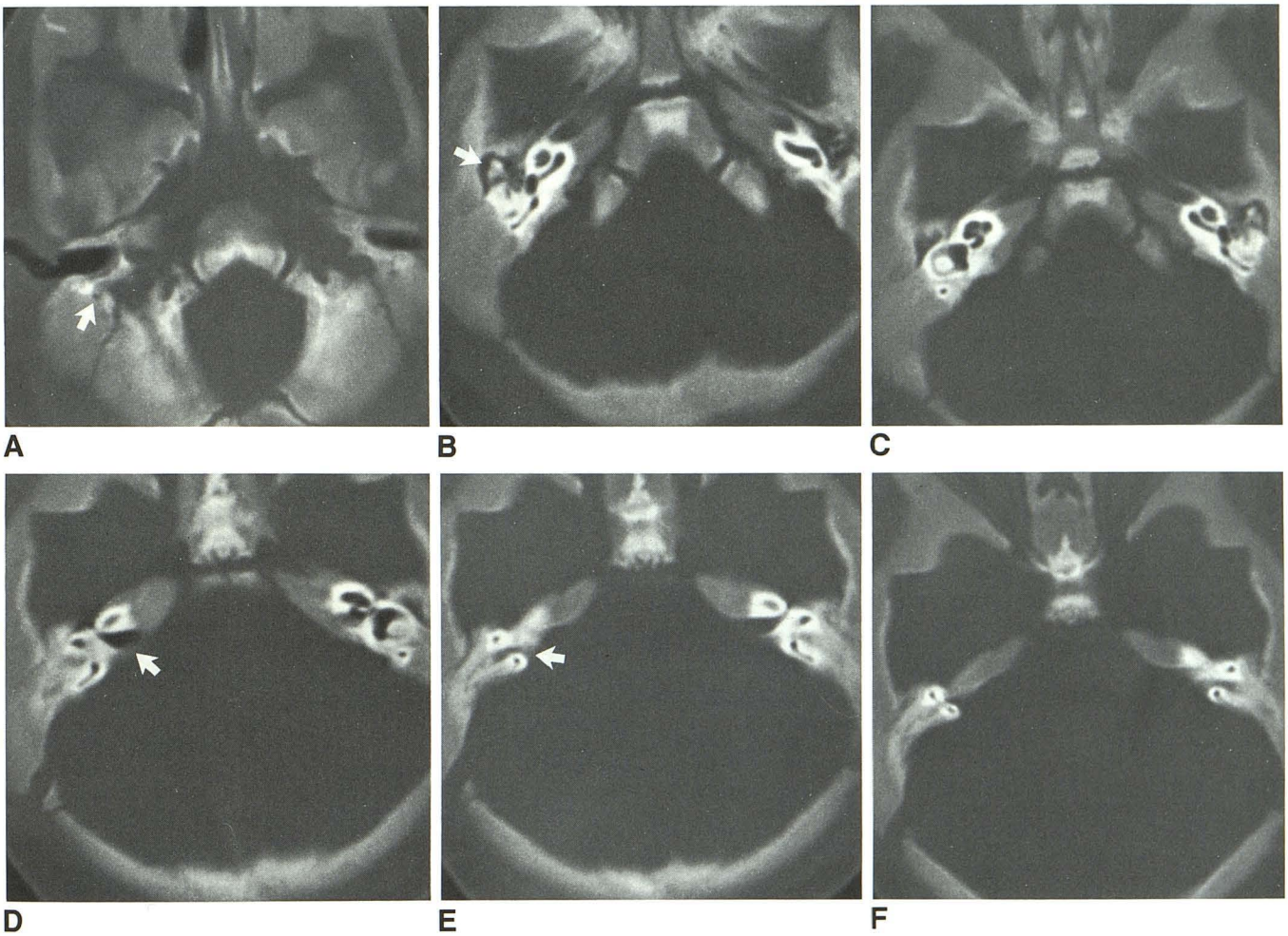

Fig. 4.—Axial images of temporal bones of case 2 at 16 months of age. Figure 5 is available for comparison.

***A*, Stylomastoid foramina are small (*arrow*).**

***B* and *C*, Epitympanum is small and aditus ad antrum is not visible. Ossicles appear normal; soft-tissue density in middle ear cavity (*arrow*) likely represents mucosal change or fluid.**

***D–F*, Internal auditory canals (*arrow* in *D*) are wide medially and narrow laterally with a short posterior wall resulting in a "fetal" trumpet shape. Prominent subarcuate fossae (*arrow* in *E*) extend into loops of superior semicircular canals.**

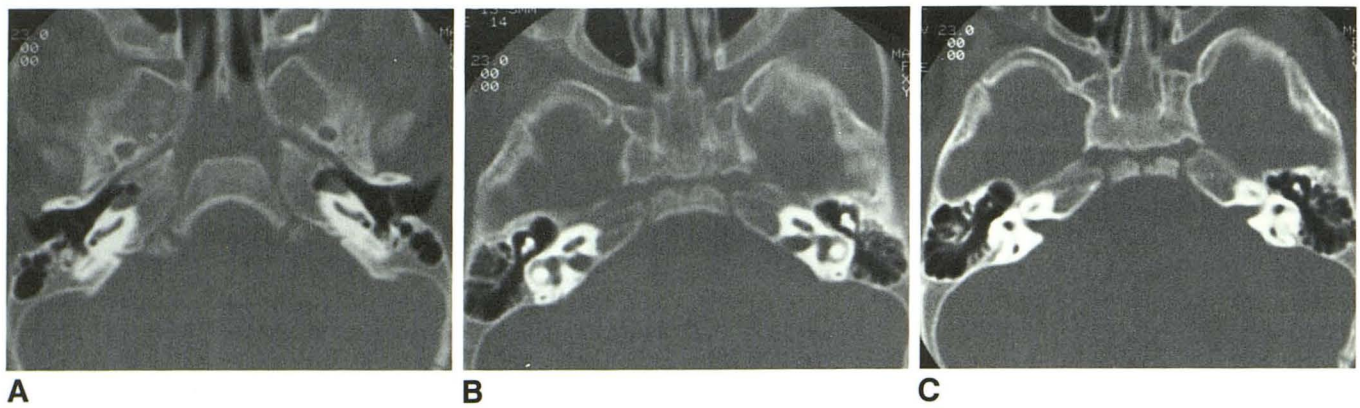

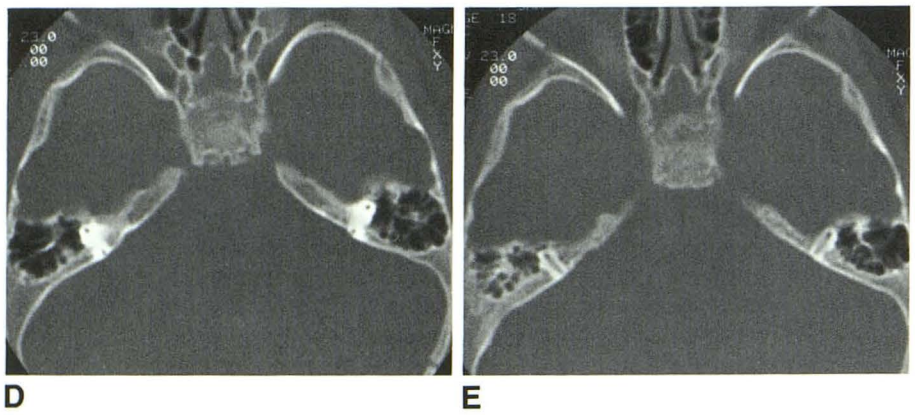

Fig. 5.—*A–E*, Axial images of normal temporal bone in 12-month-old child for comparison. Internal auditory canals are normal in shape with better development of posterior wall. Bone thickening and subarcuate fossae are not present.

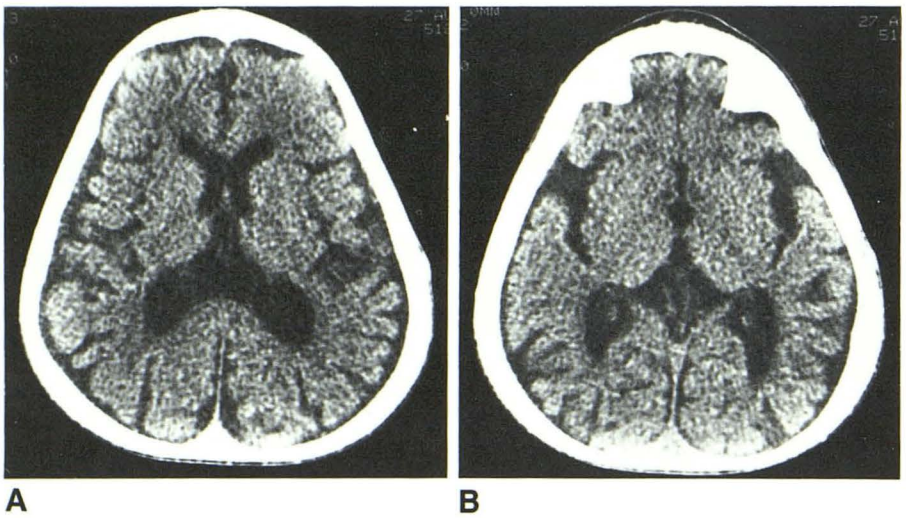

Fig. 6.—*A* and *B*, Axial images through ventricular system of case 2 at 9 months of age. Ventricles and extracerebral spaces are enlarged. Parietal bossing is present. There is no subdural collection.

4. *Skull base and calvarium*

Parietal bossing occurred in all patients with additional frontal bossing if anterior extracerebral collections were present (Figs. 2D and 6). Skull thickness increased with age along with loss of corticomedullary separation (Figs. 3A and 3B). Skull base foramina (e.g., foramen ovale) could occasionally be identified. The foramen magnum and pituitary fossa appeared normal in all patients. Pterygoid plate thickening was occasionally noted.

5. *Intracranial contents*

Five of six patients in the severe group had macrocephaly. Although one patient initially had normal-appearing CSF spaces, all six children eventually developed dilated ventricles and extracerebral spaces (Fig. 6). No signs of dural-based extramedullary hematopoiesis were seen. Reduced gray-white matter differentiation was apparent in all cases, related to immaturity in some, but likely artifactual in others as related to exaggerated beam-hardening effects.

Mild Form

Clinical

Two children had milder courses despite presentations before 3 months of age. In one infant, agammaglobulinemia and frequent infections developed. Although head circumference and bone density were increased, there was only mild anemia and no cranial nerve dysfunction as late as 23 months of age. The second child had mild anemia with occasional thrombocytopenia and macrocephaly. Recurring otitis media contributed to the abnormal auditory evoked responses, but no cranial nerve deficit was observed. Hepatosplenomegaly did not occur in either child.

Radiologic

Less dramatic radiographic findings were present, although some of the findings were characteristic of the severe form (Fig. 7). Medullary hyperdensity was seen but with better corticomedullary separation. Maxillary sinus pneumatization was absent, but development of the nasal cavity and ethmoid complex seemed normal. The bony orbit appeared normal in size and there was no exophthalmos. The optic canals were also normal.

As in the severe variant, increased head circumference with enlargement of the ventricles and extracerebral spaces was observed. One of these children, initially treated with acetazolamide, eventually required ventriculoperitoneal shunting because of symptomatic pressure. Even after reduction in size of the ventricles and extracerebral spaces, head circumference continued to increase above the 97th percentile. The internal auditory canals were small and trumpet-shaped with prominent subarcuate fossae.

Discussion

Malignant osteopetrosis is a rare abnormality of bone remodeling, the genetics of which have been extensively studied [1–3]. Previous authors [10] have suggested that mild and severe variants of the recessive form occur. In our series, all patients developed symptoms and signs before 6 months of age. While the majority developed characteristically severe foraminal and marrow-space encroachment, two infants demonstrated a distinctly milder course (mild anemia and no evidence of extramedullary hepatopoiesis). While macrocephaly with ventricular and subarachnoid space enlargement was present in both children, no cranial nerve deficit was noted at 18 and 23 months of age, respectively. Their clinical and radiologic courses support this hypothesis.

Plain film changes in osteopetrosis have been well documented [1, 3, 10], but little has been written about the detailed CT findings. The most characteristic finding in children with the severe variant is increased bone density. This is demonstrated on CT as increased medullary density with loss of trabecular definition. In children studied on multiple occasions, progressive cranial base and vault thickening was noted along with increased density of the medullary spaces. Children imaged after 1 year of age demonstrated the most obvious hyperdensity. In the extreme example, there was diffuse bone thickening with complete loss of corticomedullary demarcation (Fig. 3). This is likely the result of decreased osteoclastic activity resulting in excessively mineralized osteoid. Delay or failure in pneumatization of the paranasal sinuses and mastoids was also noted. Rudimentary ethmoid air cells were observed and, in one patient, a nonaerated mastoid sinus bud was present. Deficient sinus development in combination with increased medullary density and bone thickening produces the hyperdensity characteristically noted on plain films of the skull base.

Of particular interest are the radiographic and CT findings as related to skull base development. Although the temporal bone abnormalities may be attributed to bone thickening and encroachment, the appearance of the petrous landmarks, including the internal auditory canals and subarcuate fossae, closely resembles that of the fetus [11]. Despite normal or slightly increased globe size (and therefore, presumably orbital contents) for age, the bony orbits remain small, even in the absence of significant bone thickening (Table 2, Figs. 2 and 3). This oculoorbital disproportion suggests deficient bony

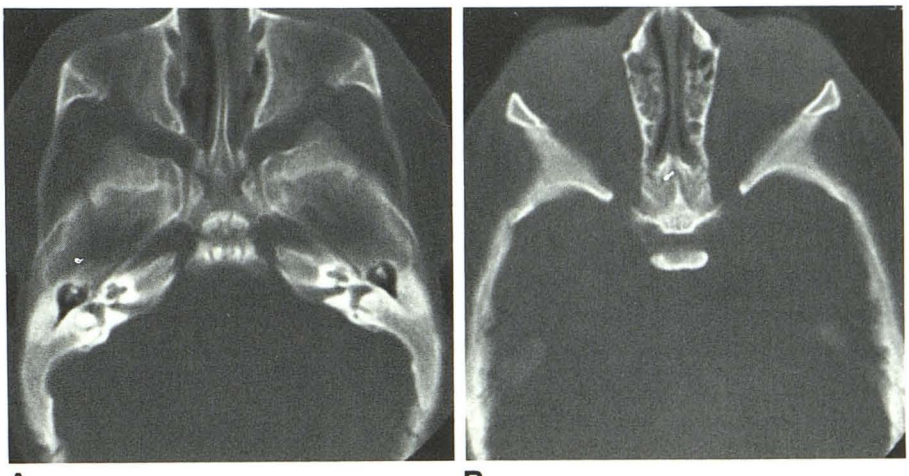

Fig. 7.—Case 8 at 23 months of age.

***A*, Axial images through temporal and facial bones show increased bone density but with better corticomedullary definition. Internal auditory canals are mildly trumpet-shaped though less than the severe variant. Maxillary sinuses and mastoid complex are not pneumatized.**

***B*, Axial image through orbits. Nasoethmoid complex is still small, but there is better ethmoid sinus development. Despite some bone thickening, optic canals are normal and proptosis is not present.**

orbital growth and development. Also, the optic canals are small even when not associated with bone wall thickening (Figs. 2 and 3). The ethmoid complex and nasal cavity were small, especially posteriorly, in addition to being underpneumatized. The fetal appearance of the temporal bone plus the small size of the orbit, optic foramina, nasal cavity, and ethmoid complex, in the absence of excessive bone thickening, suggests that deficient growth and development of the skull base is an important feature of osteopetrosis. Previous authors have suggested persistence of the "fetal state" with identification of the embryonic mesenchyme in the aditus ad antrum and fossa incudis [2] and a fetal shape to the stapes [12]. Persistence of the "fetal state" may also account for the lack of sinus and mastoid pneumatization as well as association of a small nasoethmoid complex and widened interorbital distance. The nasoethmoid complex develops from enchondral bone in the skull base [13]. Orbital position and, therefore, interorbital distance are determined by the development and medial expansion of the maxillary swellings [14]. If skull development is delayed, one would expect a small, immature nasoethmoid complex along with incomplete medial migration of the orbits and resultant wide interorbital distance. Adequate osteoid turnover is likely necessary for the proper time course in development of these structures. The immature nasoethmoid complex along with increased interorbital distance anteriorly (hypertelorism) accounted for the impression of an accentuated angle of the orbital axes.

Although auditory evoked potentials were of limited use in these patients, visual evoked responses correlated well with the clinical impression of visual impairment. Correlation with optic canal size was unreliable. All children with the severe variant demonstrated decreased canal diameters but only three had clinical blindness or optic atrophy. All these observations suggest that skull base development may be arrested or delayed while that of the cranial nerves, in addition to that of the globe, continue to follow brain growth and development [15]. This is further supported by the observations that visual impairment and proptosis developed in later infancy. Although most of the patients in this series received hormonal manipulation or marrow transplantations, limited follow-up CT scans failed to demonstrate any change.

Ventricular and extracerebral space enlargement was a frequent finding in these patients. It is speculated that impaired CSF absorption may occur secondary to primary arachnoid granulation dysfunction, dural thickening as related to extramedullary hematopoiesis, occasional subarachnoid hemorrhage, or jugular foraminal venous obstruction that produces communicating (external) obstructive hydrocephalus and macrocephaly. Of further significance were cases 4 and 8. In the former, increased head circumference was initially noted but with normal CSF spaces on CT. In the latter, the ventricles were initially dilated. Shunting led to normalization of ventricular size, but the head circumference continued above the 95th percentile. These observations seem to indicate that megacephaly may be another related manifestation.

The clinical and radiographic characteristics of our patients support the theory that there are severe and mild variants of autosomal recessive osteopetrosis. The CT appearance of the skull base suggests hypoplasia in addition to any overgrowth with small orbits, immature ethmoid and maxillary sinuses, fetal appearance to the petrous bone, and poor mastoid development. Progressive bone thickening is seen in the membranous and enchondral bones of the skull as well as a general increase in bone density, likely due to reduced osteoid resorption. CT is an excellent technique for evaluating the bone alterations in osteopetrosis in addition to the intracranial complications.

REFERENCES

1. Beighton P, Horan F, Hamersma H. A review of the osteopetroses. *Postgrad Med J* **1977**;53:507–515
2. Hawke M, Jahn AF, Bailey D. Osteopetrosis of the temporal bone. *Arch Otoloryngol* **1981**;107:278–282
3. Loria-Cortes R, Quesada-Calvo E, Cordero-Chaverri C. Osteopetrosis in children. A report of 26 cases. *J Pediatr* **1977**;91:43–47
4. Key L, Carnes D, Cole S, Holtrop M, et al. Treatment of congenital osteopetrosis with high-dose calcitriol. *N Engl J Med* **1984**;310:409–415
5. Coccia PF, Kriuit W, Cervenka J, et al. Successful bone marrow transplantation for infantile malignant osteopetrosis. *N Engl J Med* **1980**;302:701–708
6. Meschan I. *An atlas of anatomy basic to radiology*. Philadelphia: Saunders, **1975**:300–304
7. Warwick R., ed. *Eugene Wolf's anatomy of the eye and orbit*. Philadelphia: Saunders, **1975**:459
8. Warwick R., ed. *Eugene Wolf's anatomy of the eye and orbit*. Philadelphia: Saunders, **1975**:19
9. Duke-Elder S, Wybar KC. *System of ophthalmology, vol II: Anatomy of the visual system*. St. Louis: Mosby, **1961**:81
10. Neimann N, Pierson M, Marchal P, Michaud C. Evolution et pronostic de la forme precocee et grave de la maladie d'Albers-Schonberg. *Pediatrie* **1964**;19:293–307
11. Kier EL. Fetal skull (Figure 7-5). In: Newton TH, Potts DG, eds. *Radiology of the skull and brain*. St. Louis: Mosby, **1974**:103
12. Myers EN, Stool S. The temporal bone in osteopetrosis. *Arch Otolaryngol* **1969**;89:44–53
13. Langman J. *Medical embryology. Skeletal system*, 4th ed. Baltimore: Williams & Wilkins, **1981**:125–126
14. Langman J. *Medical embryology. Head and neck*, 4th ed. Baltimore: Williams & Wilkins, **1981**:283–284
15. Warwick R, ed. *Eugene Wolf's anatomy of the eye and orbit*. Philadelphia: Saunders, **1975**:460